BNL-222168-2021-TECH

EIC-ADD-TN-021

3D Theoretical and simulation tools for microbunched cooling

P. Baxevanis

September 2021

Electron-Ion Collider Project

Brookhaven National Laboratory

U.S. Department of Energy

USDOE Office of Science (SC), Nuclear Physics (NP) (SC-26)

Notice: This technical note has been authored by employees of Brookhaven Science Associates, LLC under Contract No.DE-SC0012704 with the U.S. Department of Energy. The publisher by accepting the technical note for publication acknowledges that the United States Government retains a non-exclusive, paid-up, irrevocable, world-wide license to publish or reproduce the published form of this technical note, or allow others to do so, for United States Government purposes.

DISCLAIMER

This report was prepared as an account of work sponsored by an agency of the United States Government. Neither the United States Government nor any agency thereof, nor any of their employees, nor any of their contractors, subcontractors, or their employees, makes any warranty, express or implied, or assumes any legal liability or responsibility for the accuracy, completeness, or any third party's use or the results of such use of any information, apparatus, product, or process disclosed, or represents that its use would not infringe privately owned rights. Reference herein to any specific commercial product, process, or service by trade name, trademark, manufacturer, or otherwise, does not necessarily constitute or imply its endorsement, recommendation, or favoring by the United States Government or any agency thereof or its contractors or subcontractors. The views and opinions of authors expressed herein do not necessarily state or reflect those of the United States Government or any agency thereof.

3D theoretical and simulation tools for microbunched cooling

Panagiotis Baxevanis

I. INTRODUCTION

The concept of microbunched electron cooling (MBEC, introduced in Ref. [1]) is currently under investigation as a candidate for the strong hadron cooling (SHC) component of EIC. Most of the theoretical treatments of this scheme are based on a simplified model for the longitudinal space charge [2–4]. In this model, the particle beams are treated as collections of thin charged disks, with the interaction function for two such disks being calculated by averaging the forces between constituent point charges. Although the disk model is flexible and captures a large part of the underlying physics, it lacks the fidelity and robustness of an analysis that explicitly treats the beams as collections of point charges. In what follows, we explore such a model, both from a theory-based and a simulation perspective.

II. 3D SIMULATION ALGORITHM

In this section, our objective is to describe a simple algorithm for the three-dimensional simulation of MBEC. In view of the localized nature of the space charge interaction - the key effect behind the cooling - we can focus our attention on a relatively small longitudinal part (or slice) of the beam. Within such a slice (the typical length of which is $\sim \Sigma/\gamma$, where Σ is the transverse beam size and γ is the relativistic factor), beam parameters such as current and emittance may be considered as constant. Adopting a macroparticle model for both the hadron and the electron beams, we associate to each macroparticle a phase-space coordinate vector $(x, y, z, p_x, p_y, \eta)$, all quantities being measured in the lab frame. In particular, (x, y) are the transverse position coordinates, $z = z_{lab} - v_0 t$ is the longitudinal position with respect to the beam centroid, $(p_x, p_y) = (dx/ds, dy/ds)$ are the transverse momenta (with $s = v_0 t = c\beta_0 t$) and $\eta = \gamma/\gamma_0 - 1$ is the fractional energy deviation (for future reference, we also note that $\beta_0 = (1 - 1/\gamma_0^2)^{1/2} \approx 1 - 1/(2\gamma_0^2)$). All the phase space coordinates are considered to be unconstrained quantities except for the internal bunch position z, for which we assume periodic boundary conditions within a suitable interval $(-L/2, L/2)$, i.e. $z(s + L) = z(s)$. Moreover, whereas all the other variables are typically drawn from normal (that is, Gaussian) distributions, we use a uniform distribution in order to initialize z.

Next, we comment on how to efficiently calculate the longitudinal space charge force experienced by a particle within the above-mentioned slice, a key component of our simulation

algorithm. Assuming - for the time being - that only one species of particles is present (for instance, only the electrons), the longitudinal space charge force is

$$F_i \propto e^2 \sum_j \Phi(x_i - x_j, y_i - y_j, z_i - z_j)\,, \tag{1}$$

where e is the electron charge, (x_i, y_i, z_i) are the electron macroparticle positions and $\Phi(x, y, z)$ is the particle-to-particle interaction function, which is given by

$$\Phi(x, y, z) = \frac{\gamma_0 z}{(x^2 + y^2 + \gamma_0^2 z^2)^{3/2}}\,. \tag{2}$$

This expression can be justified as follows: in the *beam frame*, any two point charges (i.e. electrons, labeled here by i and j) are at rest. As a result, their interaction is purely through the Coulomb force. By Lorentz-transforming the z-component of the electrostatic field back to the *lab frame*, one readily arrives at the results mentioned above.

The proportionality sign in the relation for the space charge force is due to the difference between actual particles and simulation macroparticles. Although the latter are assumed to have the same charge and mass as their real counterparts, they are typically much fewer in number and are only meant as a device that approximates the average quantities of the beam. Thus, if the sum was supposed to extend over all the actual particles of the beam, the proportionality constant would be equal to unity. However, when one deals with macroparticles, the above-mentioned constant needs to be set equal to $N_e/N_{e,m}$, where N_e is the total number of electrons in the slice and $N_{e,m}$ is the number of electron macroparticles.

Calculating this force through direct summation of interaction pairs can be prohibitively time-consuming, as the computation time scales like the square of the number of macroparticles. Instead, we employ the following procedure: Introducing the volume density

$$n(x, y, z) = \sum_j \delta(x - x_j)\delta(y - y_j)\delta(z - z_j), \tag{3}$$

we can express the force on the individual macroparticles as $F_i = F(x_i, y_i, z_i)$, where

$$F(x, y, z) \propto e^2 \int dx'dy'dz' \Phi(x - x', y - y', z - z') n(x', y', z')\,. \tag{4}$$

As a result of this manipulation we deduce that the function F is proportional to the three-dimensional convolution of the electron density with the space charge interaction function. To exploit this observation, we define a rectangular grid (x_G, y_G, z_G) that encompasses the

entire beam and calculate both Φ and n at the grid points (the latter requires a routine to count particles in a subdivided space, very much like a 3D histogram). Having thus discretized Φ and n in the form of three-dimensional arrays, we can use existing, FFT-based routines in order to calculate their convolution and determine F at the cartesian grid points. Finally, knowing F as a 3D array, we can readily obtain the original force components F_i through interpolation at the macroparticle locations. This technique yields sufficiently accurate results and scales much more favorably with the number of particles (indeed, the computation time is roughly proportional to the total number of *bins* into which the slice is subdivided).

Given the above, it is straightforward to write down the equations of motion for a single electron under the influence of the space charge force of the e-beam alone (as is the case in the amplification sections of the MBEC lattice). For the longitudinal portion of the motion, we start from the definition of z to obtain

$$\frac{dz}{dt} = c(\beta_z - \beta_0) \approx \frac{c}{2}(\frac{1}{\gamma_0^2} - \frac{1}{\gamma^2} - \beta_x^2 - \beta_y^2)\,, \tag{5}$$

where we have used the approximation $\beta_z \approx 1-(1/2)(1/\gamma^2+\beta_x^2+\beta_y^2)$ for the scaled velocity component along the z-direction. Taking into account that $\gamma = \gamma_0(1+\eta)$ and $\beta_{x,y} \approx p_{x,y}$, we have

$$\frac{dz}{ds} \approx \frac{\eta}{\gamma_0^2} - \frac{1}{2}(p_x^2 + p_y^2)\,, \tag{6}$$

with the term $\propto 1/\gamma_0^2$ representing the R_{56} of the drift, while the quadratic term gives the contribution of the transverse velocity components.

At this point, it is useful to divert somewhat so as to discuss the *transverse* motion of the electrons. Our basic assumption is that the transverse dynamics is predominantly determined by the focusing lattice, with the transverse space charge forces being small in comparison. We can further simplify our analysis by adopting the so-called smooth focusing approximation, in which the electrons execute harmonic betatron oscillations according to $d^2x/ds^2 + k_\beta^2 x = 0$ and $d^2y/ds^2 + k_\beta^2 y = 0$, where k_β is the focusing strength (assumed the same in both x and y). This approximation is valid so long as the lattice beta function does not vary greatly over the length of a focusing cell (alternatively, one may require that the betatron phase advance per cell be much smaller than unity). Moreover, the focusing strength is given by $k_\beta = 1/\beta_{av}$, where β_{av} is the average lattice beta function. A beam matched to this smooth focusing channel has an rms size $\Sigma_p = \sqrt{\epsilon\beta_{av}}$ and divergence

$\Sigma'_p = \sqrt{\epsilon/\beta_{av}}$, where ϵ is the transverse emittance. Summarizing, we conclude that the transverse motion of the *i-th* electron is governed by

$$\frac{dx_i}{ds} = p_{x,i} \; , \frac{dp_{x,i}}{ds} = -k_\beta^2 x_i \, , \tag{7}$$

$$\frac{dy_i}{dt} = p_{y,i} \; , \frac{dp_{y,i}}{ds} = -k_\beta^2 y_i \, . \tag{8}$$

In the context of the smooth focusing approximation introduced above, it can be shown that the z-equation of motion becomes

$$\frac{dz_i}{ds} \approx \frac{\eta_i}{\gamma_0^2} - \frac{1}{2}(p_{x,i}^2 + p_{y,i}^2 + k_\beta^2(x_i^2 + y_i^2)) \, . \tag{9}$$

Lastly, the remaining part of the longitudinal equations of motion governs the electron energy change due to the space charge interaction. Starting from $m_e c^2 d\gamma_i/ds \approx F_i$, we readily obtain

$$\frac{d\eta_i}{ds} = \frac{F_i}{\gamma_0 m_e c^2} = \frac{e^2}{\gamma_0 m_e c^2} \frac{N_e}{N_{e,m}} \sum_j \Phi(x_i - x_j, y_i - y_j, z_i - z_j) \, , \tag{10}$$

where the sum on the RHS is to be calculated via the 3D convolution technique discussed earlier in the text. In doing so, a very important caveat is that the density quantity to be convolved with the interaction function Φ is actually the *perturbed* volume density $\delta n = n - n_{\text{back}}$, which is obtained after subtracting the background component n_{back} from the calculated total density n. This manipulation is required in order to remove the DC electric field component of the slice and focus on the portion that drives the plasma oscillations.

Eqs. (7)-(10) define the model we rely on for three-dimensional simulations of the electron beam, as it propagates through the drift spaces in the amplification sections. As for going through a chicane, we use a simple linear transfer map of the form $z_2 = z_1 + R_{56}\eta_1$, all other phase space variables being considered unchanged by the passage. This is an approximation that can justified for a relatively short chicane; a more realistic linear transfer matrix can also be used if needed. Such a symplectic, potentially 6D map is - in general - necessary in order to accurately model the hadron transfer line between modulator and kicker, taking full account of the lattice dynamics (including dispersion and phase advance).

As far as the modulator and kicker sections are concerned, we assume that the plasma oscillations in the electron beam can be disregarded, which is reasonable as long as the electron quarter plasma period is comfortably larger than the modulator/kicker lengths $L_{m,k}$.

For the hadrons, plasma effects are always negligible due to the much larger mass. Short M/K sections also allow us to neglect the size variations of the unfocused, co-propagating hadron and electron beams (in effect, neglecting the impact of the angular spread). As a result, we may focus exclusively on the energy change imparted by the hadrons to the electrons and vice versa. These are expressed by

$$\Delta\eta_i = -\frac{Ze^2 L_m}{\gamma_0 m_e c^2}\frac{N_h}{N_{h,m}}\sum_j \Phi(x_i - x_j^{(h)}, y_i - y_j^{(h)}, z_i - z_j^{(h)})\,, \tag{11}$$

and

$$\Delta\eta_i^{(h)} = -\frac{Ze^2 L_k}{\gamma_0 m_h c^2}\frac{N_e}{N_{e,m}}\sum_j \Phi(x_i^{(h)} - x_j, y_i^{(h)} - y_j, z_i^{(h)} - z_j)\,, \tag{12}$$

respectively. Here, Ze, m_h and N_h are the charge, mass and total number of the hadrons, while $N_{h,m}$ is the number of hadron macroparticles.

One final point needs to be clarified regarding the transition stages between M/K and the amplification sections. These two parts of the MBEC lattice are characterized by considerably different electron beam transverse sizes. This "squeezing" of the electrons in the amplifiers is, of course, necessary in order to augment the bunching and ensure efficient cooling. The actual beam line sections that accomplish the squeeze are approximated by a map of the form $(x, y)_2 = r_p(x, y)_1$, $(p_x, p_y)_2 = (1/r_p)(p_x, p_y)_1$ - with r_p being the size squeeze factor - while the longitudinal coordinates (z, η) are unaltered. This simplified map preserves the transverse emittance of the electron beam and accounts for the different beam sizes.

The computational techniques we have just finished outlining contain most of the basic physics of MBEC in the full, three-dimensional regime. As such, they form a versatile toolkit that can be used for calculating both the cooler wakefields and the cooling times.

III. THEORETICAL ANALYSIS

The simulation algorithm described in the previous section can be benchmarked and complemented through comparison with theory. To start with, we consider the problem of 3D plasma oscillations in a "parallel" electron beam of finite transverse size, neglecting the impact of angular spread and focusing. While not very useful for practical purposes, this limiting case offers an instructive, idealized model that can be treated quasi-analytically

in a relatively straightforward manner. Recalling our earlier discussion of single particle dynamics, the equations of motion for an electron in a parallel beam may be written as

$$\frac{dz}{ds} = \frac{\eta}{\gamma_0^2}\,, \tag{13}$$

$$\frac{d\eta}{ds} = \frac{e^2}{\gamma_0 m_e c^2}\int dx'dy'dz'\delta n(x',y',z';s)\Phi(x-x',y-y',z-z')\,, \tag{14}$$

where δn is the perturbation of the electron beam volume density. As we have noted before, these equations incorporate the energy modulation due to the space charge interaction, as well as the natural chicane strength of the drift. The distribution function F for the electron beam can be decomposed as

$$F(x,y,z,\eta;s) = n_0 F_0(x,y,\eta) + \delta F(x,y,z,\eta;s)\,, \tag{15}$$

where n_0 is the background *line* density of the beam,

$$F_0 = \frac{1}{(2\pi)^{3/2}\Sigma_p^2\sigma_e}\exp(-\frac{x^2+y^2}{2\Sigma_p^2})\exp(-\frac{\eta^2}{2\sigma_e^2})\,, \tag{16}$$

(where Σ_p is the rms size of the round beam and σ_e is the rms energy spread) and δF is a small perturbation, which can be liked to δn via

$$\delta n(x,y,z;s) = \int d\eta \delta F(x,y,z,\eta;s)\,. \tag{17}$$

The self-consistent evolution of the electron beam distribution function is governed by the Vlasov equation, i.e.

$$\frac{\partial F}{\partial s} + \frac{dz}{ds}\frac{\partial F}{\partial z} + \frac{d\eta}{ds}\frac{\partial F}{\partial \eta} = 0\,, \tag{18}$$

the first-order (linearized) component of which can be written as

$$\frac{\partial(\delta F)}{ds} + \frac{\eta}{\gamma_0^2}\frac{\partial(\delta F)}{dz} + n_0\frac{e^2\mathcal{E}(x,y,z;s)}{\gamma_0 m_e c^2}\frac{\partial F_0}{d\eta} = 0\,, \tag{19}$$

where

$$\mathcal{E}(x,y,z;s) = \int dx'dy'dz'\delta n(x',y',z';s)\Phi(x-x',y-y',z-z')\,. \tag{20}$$

Introducing the Fourier quantities $\delta\hat{F}_z$ and $\hat{\mathcal{E}}_z$ via the definitions

$$\delta F(x,y,z,\eta;s) = \frac{1}{2\pi}\int dk_z \delta\hat{F}_z(x,y,k_z,\eta;s)\exp(ik_z z)\,, \tag{21}$$

$$\mathcal{E}(x,y,z;s) = \frac{1}{2\pi}\int dk_z \hat{\mathcal{E}}_z(x,y,k_z;s)\exp(ik_z z)\,, \tag{22}$$

the frequency-domain, linearized Vlasov equation becomes

$$\frac{\partial(\delta\hat{F}_z)}{ds} + \frac{\eta}{\gamma_0^2} ik_z \delta\hat{F}_z + n_0 \frac{e^2 \hat{\mathcal{E}}_z}{\gamma_0 m_e c^2} \frac{\partial F_0}{d\eta} = 0\,. \tag{23}$$

The solution of this first-order differential equation is

$$\begin{aligned} \delta\hat{F}_z(x,y,k_z,\eta;s) &= \delta\hat{F}_z(x,y,k_z,\eta;0)\exp(-i\eta k_z s/\gamma_0^2) \\ &- n_0 \frac{e^2}{\gamma_0 m_e c^2} \frac{\partial F_0}{d\eta} \int_0^s ds' \hat{\mathcal{E}}_z(x,y,k_z;s')\exp(i\eta k_z(s'-s)/\gamma_0^2)\,. \end{aligned} \tag{24}$$

In the above equations only the longitudinal wavenumber k_z is present. Next, we introduce the *full* Fourier space quantities $\delta\hat{F}_{\mathbf{k}}$ and $\hat{\mathcal{E}}_{\mathbf{k}}$ via

$$\delta\hat{F}_{\mathbf{k}} = \int d^2\mathbf{x} \exp(-i\mathbf{k}_\perp \cdot \mathbf{x}) \delta\hat{F}_z = \int d^2\mathbf{x} dz \exp(-i\mathbf{k}_\perp \cdot \mathbf{x} - ik_z z)\delta F \tag{25}$$

and

$$\hat{\mathcal{E}}_{\mathbf{k}} = \int d^2\mathbf{x} \exp(-i\mathbf{k}_\perp \cdot \mathbf{x}) \hat{\mathcal{E}}_z = \int d^2\mathbf{x} dz \exp(-i\mathbf{k}_\perp \cdot \mathbf{x} - ik_z z)\mathcal{E}\,, \tag{26}$$

where $\mathbf{x} = (x, y)$ is the transverse position and $\mathbf{k}_\perp = (k_x, k_y)$ is the transverse wavenumber vector. In a similar way, the corresponding Fourier transform of the density perturbation $\delta n(\mathbf{x}, z)$ is defined by

$$\delta\hat{n}_{\mathbf{k}} = \int d^2\mathbf{x} dz \exp(-i\mathbf{k}_\perp \cdot \mathbf{x} - ik_z z)\delta n \tag{27}$$

and also satisfies the relations

$$\delta\hat{n}_{\mathbf{k}} = \int d\eta \delta\hat{F}_{\mathbf{k}} \tag{28}$$

and

$$\hat{\mathcal{E}}_{\mathbf{k}} = -\frac{4\pi i k_z \delta\hat{n}_{\mathbf{k}}}{k_z^2 + \gamma_0^2(k_x^2 + k_y^2)}\,. \tag{29}$$

In order to derive the latter equation, one needs to recall the convolution-type definition of $\mathcal{E}$ and review the Fourier transform for the Coulomb field. Using all of the above, it is straightforward to obtain a single equation for $\delta\hat{n}_{\mathbf{k}}$ (after some lengthy Gaussian integration). The end result is

$$\begin{aligned} \delta\hat{n}_{\mathbf{k}}(s) &= \int d\eta \delta\hat{F}_{\mathbf{k}}(0)\exp(-i\eta k_z s/\gamma_0^2) + \frac{e^2 n_0 k_z^2}{\pi\gamma_0^3 m_e c^2} \int_0^s ds'(s'-s) \\ &\times \exp(-\sigma_e^2(s'-s)^2 k_z^2/(2\gamma_0^4)) \int d^2\mathbf{k}'_\perp \frac{\exp(-\Sigma_p^2({k'_x}^2 + {k'_y}^2)/2)\delta\hat{n}_{\mathbf{k}_\perp - \mathbf{k}'_\perp, k_z}(s')}{k_z^2 + \gamma_0^2((k_x - k'_x)^2 + (k_y - k'_y)^2)}\,. \end{aligned} \tag{30}$$

For the special case in which $\sigma_e \to 0$ and $\delta\hat{F}_{\mathbf{k}}(0) \propto \delta(\eta)$, we can simplify our expression by differentiating twice over s. This eliminates the integral over s' and leads to the following equation governing the 3D plasma oscillations in a *cold electron beam*:

$$\frac{\partial^2 \delta\hat{n}_{\mathbf{k}}(s)}{\partial s^2} = -\frac{e^2 n_0 k_z^2}{\pi\gamma_0^3 m_e c^2} \int d^2\mathbf{k}'_\perp \frac{\exp(-\Sigma_p^2({k'_x}^2 + {k'_y}^2)/2)\delta\hat{n}_{\mathbf{k}_\perp - \mathbf{k}'_\perp, k_z}(s)}{k_z^2 + \gamma_0^2((k_x - k'_x)^2 + (k_y - k'_y)^2)}\,, \tag{31}$$

which can also be re-written as

$$\begin{aligned}
\frac{\partial \delta\hat{n}_{\mathbf{k}}(s)}{\partial s} &= \delta\hat{p}_{\mathbf{k}}(s)\,, \\
\frac{\partial \delta\hat{p}_{\mathbf{k}}(s)}{\partial s} &= -\frac{e^2 n_0 k_z^2}{\pi\gamma_0^3 m_e c^2} \int d^2\mathbf{k}'_\perp \frac{\exp(-\Sigma_p^2({k'_x}^2 + {k'_y}^2)/2)\delta\hat{n}_{\mathbf{k}_\perp - \mathbf{k}'_\perp, k_z}(s)}{k_z^2 + \gamma_0^2((k_x - k'_x)^2 + (k_y - k'_y)^2)}\,.
\end{aligned} \tag{32}$$

This equation can be solved numerically using any of the standard techniques along with a routine for the calculation of the 2D convolution integral on the RHS. We note that, unlike the longitudinal wavenumber k_z (which essentially acts as a free parameter), the transverse wavenumbers are coupled, a fact that stems from the non-uniformity of the electron beam density in the transverse plane.

A useful corollary of the analysis presented above is related to the propagation of $\delta\hat{n}_{\mathbf{k}}$ through a chicane with strength R_{56} following a drift of length L_d. Specifically, a coordinate transformation of the form $z \to z' = z + R_{56}\eta$, $\eta \to \eta' = \eta$ modifies the beam distribution function according to

$$F(z, \eta) \to F(z - R_{56}\eta, \eta)\,. \tag{33}$$

This property reflects the fact that the distribution function is constant along a phase space trajectory. As a consequence, the Fourier component $\delta\hat{F}_{\mathbf{k}}$ is shifted according to

$$\delta\hat{F}_{\mathbf{k}} \to \delta\hat{F}_{\mathbf{k}} \exp(-ik_z R_{56}\eta)\,. \tag{34}$$

Combining this result with the derivation that led to Eq. (30), we ultimately find that the value of $\delta\hat{n}_{\mathbf{k}}$ after the chicane is given by

$$\begin{aligned}
\delta\hat{n}^+_{\mathbf{k}}(L_d) &= \int d\eta \delta\hat{F}_{\mathbf{k}}(0) \exp(-i\eta k_z(L_d/\gamma_0^2 + R_{56})) \\
&+ \frac{e^2 n_0 k_z^2}{\pi\gamma_0^3 m_e c^2} \int_0^{L_d} ds'(s' - L_d - \gamma_0^2 R_{56}) \exp(-\sigma_e^2((s' - L_d)/\gamma_0^2 - R_{56})^2 k_z^2/2) \\
&\times \int d^2\mathbf{k}'_\perp \frac{\exp(-\Sigma_p^2({k'_x}^2 + {k'_y}^2)/2)\delta\hat{n}_{\mathbf{k}_\perp - \mathbf{k}'_\perp, k_z}(s')}{k_z^2 + \gamma_0^2((k_x - k'_x)^2 + (k_y - k'_y)^2)}\,.
\end{aligned} \tag{35}$$

For a cold beam, this simplifies to

$$\begin{aligned}\delta\hat{n}^{+}_{\mathbf{k}}(L_d) &= \delta\hat{n}_{\mathbf{k}}(0) + \frac{e^2 n_0 k_z^2}{\pi\gamma_0^3 m_e c^2}\int_0^{L_d} ds'(s' - L_d - \gamma_0^2 R_{56}) \\ &\times \int d^2\mathbf{k}'_\perp \frac{\exp(-\Sigma_p^2({k'_x}^2 + {k'_y}^2)/2)\delta\hat{n}_{\mathbf{k}_\perp - \mathbf{k}'_\perp, k_z}(s')}{k_z^2 + \gamma_0^2((k_x - k'_x)^2 + (k_y - k'_y)^2)} \\ &= \delta\hat{n}_{\mathbf{k}}(L_d) + \gamma_0^2 R_{56}\delta\hat{p}_{\mathbf{k}}(L_d)\,. \end{aligned} \tag{36}$$

This useful relation fits naturally with the numerical solution of Eq. (32), which simultaneously tracks both $\delta\hat{n}_{\mathbf{k}}$ and its s-derivative $\delta\hat{p}_{\mathbf{k}}$ along the drift.

To integrate our current analysis into the framework of an actual cooling system, we need an expression for the electron beam density perturbation coming out of the modulator. In what follows, we obtain such an expression using a derivation by G. Stupakov. To start with, let us denote by $\delta\hat{n}^{(M)}_{\mathbf{k}}$ the fluctuation of the hadron volume density in the modulator. Recalling Eqs. (20) and (29), we deduce that its electric field is given by

$$\hat{E}_{z,\mathbf{k}} = -\frac{4\pi Zeik_z}{\gamma_0^2(k_x^2 + k_y^2) + k_z^2}\delta\hat{n}^{(M)}_{\mathbf{k}}, \tag{37}$$

and the corresponding electron energy modulation in Fourier representation

$$\Delta\hat{\eta}^{(e)}_{\mathbf{k}} = -\frac{e\hat{E}_{z,\mathbf{k}}L_m}{m_e\gamma_0 c^2} = \frac{4\pi Ze^2 L_m ik_z}{\gamma_0^2(k_x^2 + k_y^2) + k_z^2}\frac{\delta\hat{n}^{(M)}_{\mathbf{k}}}{m_e\gamma_0 c^2}\,. \tag{38}$$

The next step is to find the perturbation of the electron beam distribution function after the particle energy is changed in the modulator and the beam passes through the first chicane $R_e = R^{(e)}_{56}$. In this calculation we neglect the change of the electron distribution function in the modulator that is due to the betatron oscillations, and also neglect fluctuations in the electron beam. With this in mind, we denote the equilibrium electron distribution function in the modulator as $F_e(x, y, p_x, p_y, \eta)$, normalized so that the integral over all the variables is equal to one. The electron density perturbation induced by $\Delta\eta^{(e)}(x, y, z)$ is

$$\begin{aligned}\delta n^{(e)}(x, y, z) &= n_0 \int dp_x\, dp_y\, d\eta\, [F_e(x, y, p_x, p_y, \eta - \Delta\eta^{(e)}(x, y, z - R_e\eta)) - F_e] \\ &\approx -n_0 \int dp_x\, dp_y\, d\eta\, \Delta\eta^{(e)}(x, y, z - R_e\eta)\, \partial_\eta F_e\,, \end{aligned} \tag{39}$$

where we do not show the arguments of F_e if they are not shifted. Defining the quantity $\mathcal{F}_e = \int dp_x\, dp_y\, F_e$, we find that

$$\delta n^{(e)}(x, y, z) = -n_0 \int d\eta\, \Delta\eta^{(e)}(x, y, z - R_e\eta)\, \partial_\eta \mathcal{F}_e(x, y, \eta)\,. \tag{40}$$

Assuming Gaussian distributions in all three variables of $\mathcal{F}_e$, i.e.

$$\mathcal{F}_e(x,y,\eta) = \frac{1}{(2\pi)^{3/2}\Sigma_x\Sigma_y\sigma_e}\exp\left(-\frac{x^2}{2\Sigma_x^2}\right)\exp\left(-\frac{y^2}{2\Sigma_y^2}\right)\exp\left(-\frac{\eta^2}{2\sigma_e^2}\right), \tag{41}$$

the corresponding Fourier pair is

$$\begin{aligned}\hat{\mathcal{F}}_{e,\mathbf{k}_\perp}(\eta) &= \int dx\,dy\,\mathcal{F}_e(x,y,\eta)e^{-i(k_x x+k_y y)} \\ &= \frac{1}{(2\pi)^{1/2}\sigma_e}\exp\left(-\frac{k_x^2\Sigma_x^2}{2}\right)\exp\left(-\frac{k_y^2\Sigma_y^2}{2}\right)\exp\left(-\frac{\eta^2}{2\sigma_e^2}\right).\end{aligned} \tag{42}$$

Denoting $\mathbf{r} = (\mathbf{x}, z)$ and recalling that

$$\begin{aligned}\Delta\eta^{(e)} &= \frac{1}{(2\pi)^{3/2}}\int d^3\mathbf{k}\exp(i\mathbf{k}\cdot\mathbf{r})\Delta\hat{\eta}_{\mathbf{k}}^{(e)}, \\ \mathcal{F}_e &= \frac{1}{2\pi}\int d^2\mathbf{k}_\perp\exp(i\mathbf{k}_\perp\cdot\mathbf{x})\hat{\mathcal{F}}_{e,\mathbf{k}_\perp},\end{aligned} \tag{43}$$

we obtain

$$\begin{aligned}\delta\hat{n}_{\mathbf{k}}^{(e)} &= -n_0\int d^3\mathbf{r}\,e^{-i\mathbf{k}\cdot\mathbf{r}}\int d\eta\,\Delta\eta^{(e)}(x,y,z-R_e\eta)\,\partial_\eta\mathcal{F}_e(x,y,\eta) \\ &= -\frac{1}{(2\pi)^5}n_0\int d^3\mathbf{r}\,e^{-i\mathbf{k}\cdot\mathbf{r}}\int d\eta\int d^3\mathbf{k}'\,\Delta\hat{\eta}_{\mathbf{k}'}^{(e)}e^{i(k_x'x+k_y'y+k_z'(z-R_e\eta))} \\ &\times\int dk_x''\,dk_y''\,\partial_\eta\hat{\mathcal{F}}_{e,\mathbf{k}_\perp''}(\eta)e^{i(k_x''x+k_y''y)}.\end{aligned} \tag{44}$$

Next, we first integrate by parts over η and then over $d^3\mathbf{r}$, a manipulation that gives us three delta functions:

$$\begin{aligned}\delta\hat{n}_{\mathbf{k}}^{(e)} &= -\frac{1}{(2\pi)^2}n_0\int d\eta\int d^3\mathbf{k}'\,\Delta\hat{\eta}_{\mathbf{k}'}^{(e)}e^{-ik_zR_e\eta} \\ &\times\int dk_x''\,dk_y''\,(ik_z'R_e)\hat{\mathcal{F}}_{e,\mathbf{k}_\perp''}(\eta)\delta(k_x-k_x'-k_x'')\delta(k_y-k_y'-k_y'')\delta(k_z-k_z').\end{aligned} \tag{45}$$

We then integrate over $d^3\mathbf{k}'$, which yields

$$\begin{aligned}\delta\hat{n}_{\mathbf{k}}^{(e)} &= -\frac{iR_e}{(2\pi)^2}n_0\int dk_x''\,dk_y''\,d\eta\,\Delta\hat{\eta}^{(e)}_{\mathbf{k}_\perp-\mathbf{k}_\perp'',\,k_z}\hat{\mathcal{F}}_{e,\mathbf{k}_\perp''}(\eta)k_ze^{-ik_zR_e\eta} \\ &= -\frac{iR_e}{(2\pi)^2}n_0\int dk_x''\,dk_y''\,\Delta\hat{\eta}^{(e)}_{\mathbf{k}_\perp-\mathbf{k}_\perp'',\,k_z}k_z\exp\left(-\frac{k_x''^2\Sigma_x^2}{2}-\frac{k_y''^2\Sigma_y^2}{2}-\frac{k_z^2(R_e\sigma_e)^2}{2}\right).\end{aligned} \tag{46}$$

Finally, by substituting Eq. (38) into the expression given above, we arrive at the desired result, namely

$$\begin{aligned}\delta\hat{n}_{\mathbf{k}}^{(e)} &= \frac{R_e}{\pi}\frac{n_0Ze^2L_m}{m_e\gamma_0c^2}\int\frac{k_z^2dk_x''\,dk_y''}{\gamma_0^2((k_x-k_x'')^2+(k_y-k_y'')^2)+k_z^2}\delta\hat{n}^{(M)}_{\mathbf{k}_\perp-\mathbf{k}_\perp'',\,k_z} \\ &\times\exp\left(-\frac{k_x''^2\Sigma_x^2}{2}-\frac{k_y''^2\Sigma_y^2}{2}-\frac{k_z^2(R_e\sigma_e)^2}{2}\right).\end{aligned} \tag{47}$$

Using Eq. (47) along with Eqs. (32) and (36), one can track the Fourier component of the electron density perturbation along the entire MBEC lattice. For purposes of comparison with simulation (and also to ensure that physically meaningful quantities are calculated) it becomes necessary to translate the frequency-domain results into their real-space counterparts. For example, a very useful metric when tracking the bunching of the electron beam is the density fluctuation ratio $S(z) = \int d^2\mathbf{x}\, \delta n(\mathbf{x}, z)/n_0$, which is ~ 1 for a nonlinear amplifier. Since the localized density fluctuation δn is related to its Fourier pair $\delta\hat{n}_{\mathbf{k}}$ via

$$\delta n = \frac{1}{(2\pi)^{3/2}} \int d^2\mathbf{k}_\perp dk_z \exp(i\mathbf{k}\cdot\mathbf{x} + ik_z z)\delta\hat{n}_{\mathbf{k}_\perp, k_z}\,, \tag{48}$$

the ratio in question is expressed by

$$S(z) = \frac{\int dk_z\, \delta\hat{n}_{\mathbf{k}_\perp = 0, k_z} \exp(ik_z z)}{2\pi n_0}\,. \tag{49}$$

Useful relations similar to the one given above can also be obtained for other important quantities such as the effective wakefield of the cooler section. However, the latter topic will be covered in a subsequent note.

IV. NUMERICAL RESULTS

Turning to a simple numerical illustration, we now consider the case in which a single, thin hadron disk of length L_h is immersed in the middle of an electron slice (i.e. at $z = 0$). The hadron density perturbation is given by

$$\delta n^{(M)}(\mathbf{x}, z) = \frac{N_h}{2\pi\Sigma_x\Sigma_y L_h} H(z) \exp(-\frac{x^2}{2\Sigma_{x,h}^2} - \frac{y^2}{2\Sigma_{y,h}^2})\,, \tag{50}$$

where N_h is the number of hadrons, $H(z)$ is a step function that is equal to unity for $-L_h/2 \le z \le L_h/2$ and zero elsewhere, and we have assumed an elliptical cross section for the disk with rms sizes $\Sigma_{x,h}$ and $\Sigma_{y,h}$ (as well as uniform line density). The corresponding frequency-domain perturbation is

$$\delta\hat{n}_{\mathbf{k}}^{(M)} = N_h \mathrm{sinc}(k_z L_h/2) \exp(-\Sigma_{x,h}^2 k_x^2/2 - \Sigma_{y,h}^2 k_y^2/2)\,, \tag{51}$$

where $\mathrm{sinc}(x) = \sin x/x$. Using the techniques described in the two previous sections (theoretical and simulation-based), we can propagate the electron beam perturbation due to the hadrons through the MBEC lattice. Here, we consider parameters that approximate the

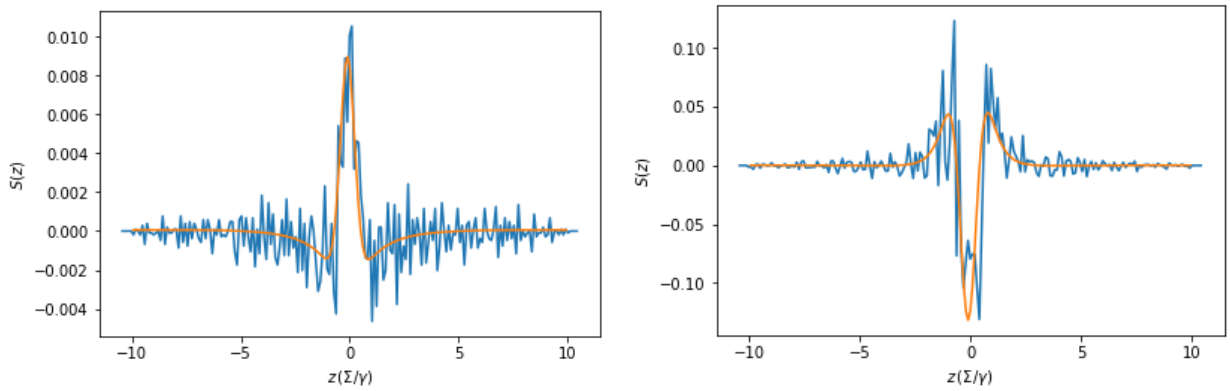


FIG. 1: Local density fluctuation ratio $S(z) = \int d^2\mathbf{x}\, \delta n(\mathbf{x}, z)/n_0$ after the first chicane (left) and after the second chicane of the cooler (right). Theory (orange plots) and simulation data (blue plots) are included.

current SHC configuration of EIC, namely: a 275 GeV proton beam, an electron beam with a peak current of $I_e = en_0c = 17\,\mathrm{A}$, a normalized transverse emittance of $\gamma_0\epsilon = 2.8\,\mu\mathrm{m}$ and an energy spread of $\sigma_e = 1 \times 10^{-4}$, a 1 m average beta function at the amplifier, $\Sigma_x = \Sigma_y = \Sigma = 0.43\,\mathrm{mm}$, $\Sigma_{x,h} = 1.1\,\mathrm{mm}$, $\Sigma_{y,h} = 0.24\,\mathrm{mm}$, $L_m = L_k = 39\,\mathrm{m}$, $L_d = 43\,\mathrm{m}$. Moreover, we have $r_p = \Sigma_p/\Sigma = 0.22$ and the chicane strengths are $R_{e,1} = R_{e,2} = 0.5\,\mathrm{cm}$ (for simplicity, only one amplification stage is assumed). As far as the simulation parameters are concerned, we have $N_e \approx 10^7$, $N_h \approx 2.5 \times 10^3$, $N_{e,m} = 2 \times 10^6$, $N_{h,m} = 2.5 \times 10^3$, $L = N_0\Sigma/\gamma_0$ with $N_0 = 20$ and $L_h = L/250$. In Fig. 1 we show the comparison between theory and simulation as far the local density ratio S is concerned. For the theory, we have utilized the cold beam model when describing the three-dimensional plasma oscillations. Furthermore, to remove a heavy noise background from the simulation results, we have subtracted the code output for the case of zero electron energy modulation (i.e. no hadrons), which allows us to focus on the coherent signal. Reasonably good agreement is observed between the two approaches and the amplification of the electron beam modulation (or bunching) is evident.

V. CONCLUSIONS

In this note, we have developed a set of fully three-dimensional simulation and theory-based techniques for the study of microbunched cooling, including the crucial effect of gain amplification. A 3D macroparticle code, along with a Vlasov equation-based, frequency-domain method, have been used to track the bunching of the electron beam along the cooler lattice. Good agreement is observed between theory and simulation, which paves the way for subsequent calculations of other key parameters, such as the effective wakefield and the cooling time scales.

---

[1] D. Ratner, Phys. Rev. Lett. **111**, 084802 (2013), URL https://link.aps.org/doi/10.1103/PhysRevLett.111.084802.

[2] G. Stupakov, Phys. Rev. Accel. Beams **21**, 114402 (2018), URL https://link.aps.org/doi/10.1103/PhysRevAccelBeams.21.114402.

[3] G. Stupakov and P. Baxevanis, Phys. Rev. Accel. Beams **22**, 034401 (2019), URL https://link.aps.org/doi/10.1103/PhysRevAccelBeams.22.034401.

[4] P. Baxevanis and G. Stupakov, Phys. Rev. Accel. Beams **22**, 081003 (2019), URL https://link.aps.org/doi/10.1103/PhysRevAccelBeams.22.081003.